Ain Shams Engineering Journal (2015) 6, 1031–1044

Ain Shams University

Ain Shams Engineering Journal

www.elsevier.com/locate/asej
www.sciencedirect.com

MECHANICAL ENGINEERING

Dynamic behavior of a rotating delaminated composite beam including rotary inertia and shear deformation effects

Ramazan-Ali Jafari-Talookolaei [a,*], Christian Della [b]

[a] School of Mechanical Engineering, Babol Noshirvani University of Technology, Shariati Av., Babol, P.O. Box: 484, Mazandaran 47148-71167, Iran[1]
[b] School of Engineering, University of Glasgow Singapore, 535 Clementi Road, Singapore 599489, Singapore

Received 21 June 2014; revised 18 February 2015; accepted 3 March 2015
Available online 4 April 2015

KEYWORDS

Rotating composite beam;
Delamination;
Vibration characteristics;
Timoshenko beam theory;
Finite element method

Abstract A finite element (FE) model is developed to study the free vibration of a rotating laminated composite beam with a single delamination. The rotary inertia and shear deformation effects, as well as the bending–extension, bending–twist and extension–twist coupling terms are taken into account in the FE model. Comparison between the numerical results of the present model and the results published in the literature verifies the validity of the present model. Furthermore, the effects of various parameters, such as delamination size and location, fiber orientation, hub radius, material anisotropy and rotating speed, on the vibration of the beam are studied in detail. These results provide useful information in the study of the free vibration of rotating delaminated composite beams.

1. Introduction

The rotating beams made of composite materials are widely used for various engineering applications, such as robotic manipulators, wind turbines, helicopter blades and aircraft propellers. The improved mechanical properties of laminated composites, such as strength-to-weight and stiffness-to-weight ratios, in comparison with the conventional metallic materials are some of the factors that have contributed to its advancement. However, composites are subjected to a wide range of damages induced during their fabrication or service life, which may significantly reduce their structural performance. One of the commonly encountered types of defects or damages in the multi-layered composite structures is delamination.

* Corresponding author. Tel./fax: +98 (111) 3210973.
E-mail addresses: ra.jafari@nit.ac.ir, ramazanali@gmail.com, rajafarit@alumni.sharif.edu (R.A. Jafari-Talookolaei), Christian.Della@glasgow.ac.uk (C. Della).
URLs: http://www.mec.nit.ac.ir/ms/ra.jafari/home.aspx, http://www.alum.sharif.ir/~rajafarit/ (R.A. Jafari-Talookolaei).
[1] URL address: http://www.en.nit.ac.ir/schools/mec/fm_Applied_Design.aspx, http://www.en.nit.ac.ir.

Peer review under responsibility of Ain Shams University.

ELSEVIER Production and hosting by Elsevier

http://dx.doi.org/10.1016/j.asej.2015.03.002

Nomenclature

L	beam length
$b \times h$	rectangular cross-section of the beam
L_1	delamination lengthwise location
L_2	delamination length
r_0	offset distance
M	end mass
J	moment of inertia of the end mass
Ω	rotating speed
h	beam thickness
h_i	thickness of the ith sub-beam
T	kinetic energy
U	potential energy
ρ_i	ith layer density
(u, w)	the LCB mid-plane displacements in the $\hat{x}$ and $\hat{y}$ directions, respectively
$(\psi_{\hat{x}}, \psi_{\hat{y}})$	the mid-plane bending slopes
$N_{\hat{x}}$	in-plane force
$(M_{\hat{x}}, M_{\hat{x}\hat{y}})$	bending and twisting moments
$Q_{\hat{x}\hat{z}}$	resultant shear force
$\varepsilon^0_{\hat{x}}$	mid-plane strain
$(\kappa_{\hat{x}}, \kappa_{\hat{x}\hat{y}})$	bending and twisting curvatures
$\varepsilon_{\hat{x}\hat{z}}$	shear strain
$\overline{A}_{ij}$	modified extensional stiffness
$\overline{B}_{ij}$	modified bending–extension coupling stiffness
$\overline{D}_{ij}$	modified bending stiffness
A_{ij}	transverse shear stiffness
F_i	centrifugal force
ω	circular frequency
k_s	shear correction factor
(A, I)	area and second moment of area, respectively
R	radius of gyration
ω_s	natural frequency of the non-rotating intact beam
E	Young Modulus
$(\eta' = \Omega L^2\sqrt{\rho A/EI}, \eta = \Omega L^2\sqrt{\rho/(E_{11}h^2)})$	dimensionless rotating speed
$(\bar{\omega}' = \omega L^2\sqrt{\rho A/EI}, \bar{\omega} = \omega L^2\sqrt{\rho/E_{11}h^2})$	dimensionless natural frequency
(e_2, e_3)	distances between the neutral axis of the sub-beams 2 and 3 with the neutral axis of the intact part, respectively
$(r = R/L, \alpha = r_0/L, \overline{L}_2 = L_2/L, \mu = M/\rho bhL, \sigma = J/\rho bhL^3)$	non-dimensional parameters used in the numerical analysis

Depending on its application, composite structures may require the use of angle ply and unsymmetrical laminates. Thus, bending–extension, bending–twist, and extension–twist coupling terms need to be considered in the analysis of composites [1–5]. Furthermore, the Poisson's effect, which is often neglected in one-dimensional laminated beam analysis, has been found to be significant in the analysis of composite beams with angle-plies and unsymmetrical layups [1–5].

Free vibration analysis of the intact rotating beams and delaminated non-rotating beams based on the classical beam theory (CBT) and the Timoshenko beam theory has received a good amount of attention in the literature [6–22]. The free vibrations of an isotropic beam with a through-width delamination by using four Euler–Bernoulli sub-beams connected at the delamination boundaries were studied by Wang et al. [6]. According to this study interpenetration of the delaminated sub-beams was seen, which was physically impossible to occur in the case of off-mid-plane delaminations. This is because the delaminated regions were assumed to deform "freely" without touching each other (free mode) and thus have different transverse deformations. To avoid this kind of incompatibility, Mujumdar and Suryanarayan [7] proposed a model in which they assumed that the delaminated layers are constrained to have identical transverse deformations, which was called the constrained mode in contrast with the free mode by Wang et al. [6]. However, the constrained mode model failed to predict the opening in the mode shapes found in the experiments by Shen and Grady [8]. Analytical and numerical solutions for beams with single and multiple delaminations have been presented by many researchers based on the CBT [9–14] and Timoshenko beam theory [15–17]. These studies emphasize on the influence of the free and constrained modes between the delaminated layers. It should be noted that the Timoshenko beam theory takes into account the shear deformation and rotary inertia effects, which are ignored in the CBT, making it suitable to study the static and dynamic behavior of thick beams. Moreover, in this case, the equation of motion is complex, and even obtaining an approximate solution is much more difficult than the CBT.

The free vibration of rotating intact beam has received considerable attention from researchers [18–22]. Kuo et al. [18] have investigated the influence of taper ratio, elastic root restraints, tip mass and rotating speed on the vibration of rotating non-uniform beams based on the CBT. Natural frequencies of rotating tapered Timoshenko beam have been presented for different combinations of the fixed, hinged and free end conditions by means of a new tapered finite beam element that accounts for the effect of shear deformation, rotary inertia, and the centrifugal stiffening due to beam rotation [19]. Du et al. [20] have presented a convergent power series expression to solve analytically for the exact natural frequencies and mode shapes of rotating Timoshenko beams. The effects of angular velocity, shear deformation and rotary inertia on the dynamic behavior of rotating beams have been evaluated. The free vibration analysis of rotating tapered beams has been investigated using the dynamic stiffness method by Su et al. [21]. The range of considered problems included beams for which the depth and/or width of the cross-section vary linearly along the length. Das et al. [22] have presented analytical solution for the free vibration of a rotating beam with nonlinear spring–mass system. The solution has been obtained by applying the method of multiple timescale directly to the nonlinear partial differential equations and the boundary conditions.

Dynamic analysis of the rotating delaminated beam has received limited attention. Recently, Liu and Shu [23] presented analytical solutions for the free vibrations of rotating isotropic beams with multiple delaminations. The Timoshenko beam theory and both the free mode and the

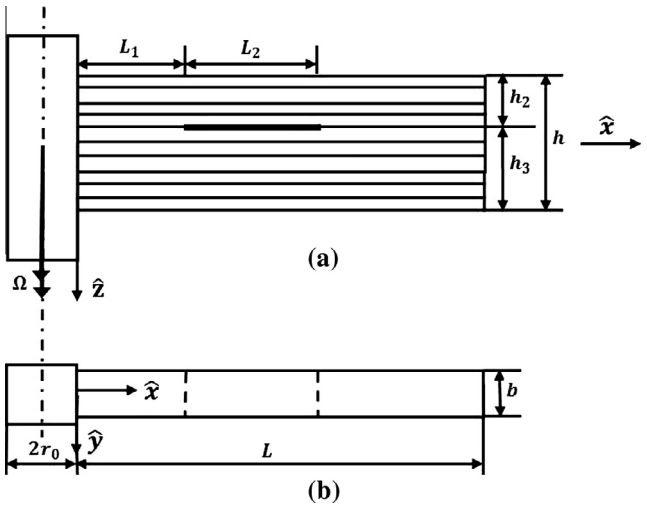

Figure 1 A schematic of generally layered composite beam with single delamination: (a) front view, and (b) top view.

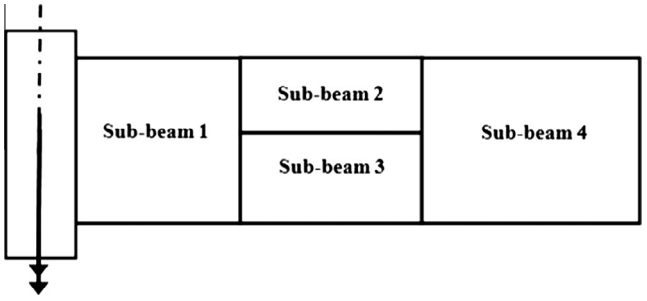

Figure 2 The delaminated beam is modeled by four interconnected sub-beams.

constrained mode assumptions in delaminated region have been used.

To the authors' best knowledge, a free vibration analysis of rotating layered composite beam (LCB) with general layups and an arbitrary delamination to include the rotary inertia and shear deformation effects, Poisson effect, and the bending–extension, bending–twist, and extension–twist coupling effects has not been presented in the literature. Therefore, the objectives of this research work were: (1) to develop a finite element model to study the free vibration of a rotating LCB with a single delamination; and (2) perform a parametric study to investigate the influence of delamination size and location, fiber orientation, hub radius, material anisotropy and rotating speed, on the free vibration of the delaminated rotating LCB.

The research is presented as follows. First, the finite element model is presented. Second, the numerical results are verified with the published analytical results on the vibration of delaminated beams and intact rotating beams. Finally, the vibration of delaminated rotating LCB is investigated.

2. Mathematical formulation

2.1. Geometrical modeling

Fig. 1 shows a laminated beam having a single delamination through the width delamination. The delamination dimension is $L_2 \times b$ and it is located at L_1 with respect to the left end of the LCB.

In order to geometrically model the LCB with a single delamination, consider Fig. 2 in which the delaminated LCB can be viewed as a combination of four intact beams (i.e. four sub-beams of 1–4) connected at the delamination boundaries $x = L_1$ and $x = L_1 + L_2$. In this way, we will have four sub-beams of 1 to 4 with lengths and thicknesses of $L_i \times h_i$ (i = 1–4) where $L_2 = L_3$, $L_4 = L$–L_1–L_2, $h_1 = h_4 = h$.

One of the efficient ways of deriving dynamic characteristics of a system is to use the finite element method (FEM). In implementing this method, one has to derive the kinetic and potential energies of the whole system to form the mass and stiffness matrices. Then, the natural frequencies and the corresponding mode shapes of the system are obtained using the eigenvalue technique. The detailed procedures are presented in the following sub-sections.

2.2. Kinetic and potential energies

The kinetic energy T of the whole beam is given by [1,3,5,16,17]

$$T = \sum_{i=1}^{4} \frac{1}{2} \int_0^{L_i} \left[I_{1,i}(u_{i,t}^2 + w_{i,t}^2) + I_{3,i}(\psi_{\hat{x}i,t}^2 + \psi_{\hat{y}i,t}^2) \right] d\hat{x} \tag{1}$$

where:

$$(I_{1,i}, I_{3,i}) = b \int_{-h_i/2}^{h_i/2} \rho_i (1, \hat{z}^2) d\hat{z} \tag{2}$$

and u and w are the LCB mid-plane displacements along the $\hat{x}$ and $\hat{z}$ directions, respectively, and $\psi_{\hat{x}}$ and $\psi_{\hat{y}}$ are the bending slopes along the $\hat{x}$ and $\hat{y}$ directions, respectively. The subscript i represents the sub-beam's number, i = 1–4 and the symbol "," used as a subscript stands for the differentiation with respect to any variable followed after it.

The potential or strain energy of the beam U is given by [16]

$$\begin{aligned} U = \sum_{i=1}^{4} \int_0^{L_i} \Bigg[& \frac{\overline{A}_{11,i}}{2} u_{i,\hat{x}}^2 + \overline{B}_{11,i} u_{i,\hat{x}} \psi_{\hat{x}i,\hat{x}} + \overline{B}_{16,i} u_{i,\hat{x}} \psi_{\hat{y}i,\hat{x}} \\ & + \overline{D}_{16,i} \psi_{\hat{x}i,\hat{x}} \psi_{\hat{y}i,\hat{x}} + \frac{\overline{D}_{11,i}}{2} \psi_{\hat{x}i,\hat{x}}^2 + \frac{\overline{D}_{66,i}}{2} \psi_{\hat{y}i,\hat{x}}^2 \\ & + \frac{\overline{A}_{55,i}}{2} (\psi_{\hat{x}i}^2 + w_{i,\hat{x}}^2 + 2\psi_{\hat{x}i} w_{i,\hat{x}}) \Bigg] d\hat{x} + \frac{1}{2} k (w_2 - w_3)^2 \\ & + \sum_{i=1}^{4} \int_0^{L_i} \frac{1}{2} F_i(\hat{x}) w_{i,\hat{x}}^2 \, d\hat{x} \end{aligned} \tag{3}$$

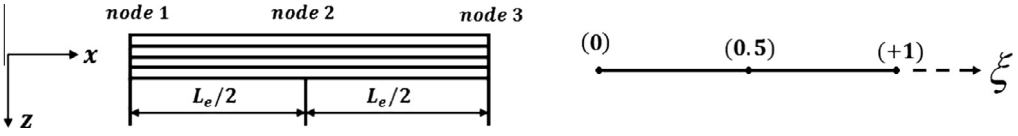

Figure 3 A three-nodded beam element and its intrinsic coordinates.

Table 1 Comparison of non-dimensional first natural frequencies of angle-ply LCB and its convergent ($L/h = 15$).

θ (°)	[25]	[5]	No. of elements							
			5	10	15	20	25	30	40	50
0	0.9820	0.979	1.0910	0.9870	0.9842	0.9787	0.9787	0.9787	0.9787	0.9787
15	0.9249	0.729	0.8134	0.7926	0.7731	0.7453	0.7249	0.7249	0.7249	0.7249
30	0.7678	0.485	0.5271	0.5043	0.4972	0.4931	0.4824	0.4824	0.4824	0.4824
45	0.5551	0.314	0.3968	0.3675	0.3341	0.3209	0.3138	0.3138	0.3138	0.3138
60	0.3631	0.263	0.3280	0.3034	0.2911	0.2798	0.2663	0.2628	0.2628	0.2628
75	0.2723	0.259	0.3176	0.2997	0.2741	0.2676	0.2602	0.2591	0.2591	0.2591
90	0.2619	0.261	0.2911	0.2863	0.2742	0.2635	0.2609	0.2609	0.2609	0.2609

Table 2 Comparison of first dimensionless frequencies of the rotating isotropic beam.

r	$\eta' = 4$			$\eta' = 8$			$\eta' = 12$	
	[20]	[23]	Present	[20]	[23]	Present	[20]	Present
0.01	5.580	5.58	5.579	9.246	9.245	9.246	13.150	13.150
0.02	5.564	5.562	5.563	9.215	9.212	9.215	13.095	13.095
0.03	5.539	5.537	5.538	9.167	9.162	9.166	13.015	13.015
0.04	5.505	5.502	5.504	9.106	9.097	9.105	12.923	12.923
0.05	5.463	5.46	5.462	9.036	9.023	9.036	12.827	12.828
0.06	5.415	5.411	5.414	8.963	8.944	8.963	12.734	12.734
0.07	5.363	5.358	5.362	8.889	8.861	8.888	12.646	12.625
0.08	5.307	5.300	5.306	8.815	8.775	8.815	12.564	12.547
0.09	5.249	5.239	5.249	8.744	8.688	8.744	12.487	12.472
0.1	5.191	5.176	5.190	8.677	8.599	8.676	12.415	12.401

Table 3 Natural frequencies (Hz) of a delaminated non-rotating beam.

Mode number	Experimental results [26]		Analytical [27]	Present
	Impulse	Sine sweep		
1st	16	17	15.73	15.45
2nd	98	99	94.86	93.65
3rd	223	223	224.77	221.08
4th	441	440	458.32	453.72

Table 4 Fundamental frequencies (Hz) of the LCB with central delamination.

$\overline{L}_2$	Present		Luo and Hanagud [28]		Shen and Grady [8]	
	Free	Cons.	Free	Cons.	Average test	Cons.
0.2	80.38	80.38	82.01	82.02	80.12	81.46
0.4	79.09	79.13	80.74	80.79	79.75	79.93
0.6	76.05	76.32	77.52	77.82	76.96	76.71
0.8	70.54	71.87	71.73	73.15	72.46	71.66

The last term represents the strain energy due to the centrifugal force F_i is [18]

$$F_i(\hat{x}) = \int_{\hat{x}}^{L} I_{1,i}\Omega^2(r_0 + \hat{x})d\hat{x} = I_{1,i}\Omega^2\left[r_0(L-\hat{x}) + \frac{L^2 - \hat{x}^2}{2}\right] \quad (4)$$

It should be noted that all of the stiffnesses $\overline{A}_{11}, \overline{B}_{11}, \overline{B}_{16}, \overline{D}_{16}, \overline{D}_{11}, \overline{D}_{66}, \overline{A}_{55}$ that are used in the potential energy in Eq. (3) are defined in Refs. [1,3,5,16,17] and will not be presented here for the sake of brevity. Moreover, referring to Eq. (3), the interaction between the delaminated sub-beams 2 and 3 (Fig. 2) can be modeled as a distributed soft spring with a stiffness of k [17] to obtain the vibration characteristics based on the constrained mode. In this way, the potential energy for the sub-beams 2 and 3 can be expressed by inclusion of this soft spring in terms of displacements. To obtain the numerical results $k = 0$ is used for the free mode and $k =$ 1e 12 for the constrained mode. In other words, for free mode there is not any restriction between sub-beams 2 and 3 in the delaminated region (free motion), whereas for the constrained mode there is a spring with large stiffness that prevents the penetration between sub-beams 2 and 3.

2.3. Element description

As shown in Fig. 3, the beam element has three nodes, and each node has four degrees of freedom, namely, u_i, w_i, ψ_{xi} and ψ_{yi} for ith node. The displacements u and w and the rotations ψ_x and ψ_y can be interpolated in terms of the intrinsic coordinate as

$$u = \sum_{i=1}^{3} N_i(\xi)u_i, \quad w = \sum_{i=1}^{3} N_i(\xi)w_i,$$
$$\psi_x = \sum_{i=1}^{3} N_i(\xi)\psi_{xi}, \quad \psi_y = \sum_{i=1}^{3} N_i(\xi)\psi_{yi} \quad (5)$$

Table 5 First two natural frequencies of the delaminated beam for different rotating speed and delamination lengths.

	$\overline{L}_2$	0.2	0.4	0.6	0.8
$\eta = 0.01$ (0.6817, 3.8750)[b]	Free	0.6816	0.6789	0.66908	0.6108
		3.8585	2.7137	1.2921	0.8025
	Cons.[a]	0.6817	0.6797	0.67587	0.6697
		3.8731	3.8579	3.8160	3.7390
$\eta = 1$ (1.2666, 4.6021)	Free	1.2666	1.2655	1.2621	1.2525
		4.5954	4.4555	3.5516	2.5808
	Cons.	1.2666	1.2659	1.2640	1.2597
		4.6003	4.4882	4.3226	4.3657
$\eta = 2$ (2.1967, 4.9852)	Free	2.1967	2.1964	2.1949	2.1889
		4.9852	4.4922	4.3230	4.3662
	Cons.	2.1967	2.1965	2.1956	2.1923
		4.9852	4.4922	4.3230	4.3662
$\eta = 3$ (3.1596, 4.9871)	Free	3.1596	3.1596	3.1590	3.1552
		4.9871	4.4928	4.3233	4.3664
	Cons.	3.1597	3.1596	3.1592	3.1567
		4.9871	4.4928	4.3234	4.3664
$\eta = 4$ (4.1322, 4.9883)	Free	4.1322	4.1315	4.1306	4.1290
		4.9883	4.4943	4.3254	4.3674
	Cons.	4.1322	4.1315	4.1307	4.1298
		4.9883	4.4943	4.3254	4.3674

[a] Constrained mode model.
[b] Number in the parenthesis indicates the non-dimensionless natural frequencies of the intact beam.

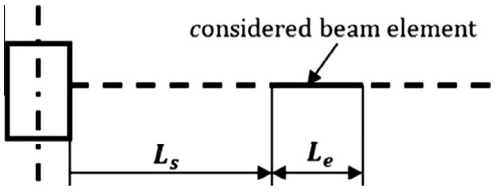

Figure 4 Location of the Timoshenko beam element under consideration.

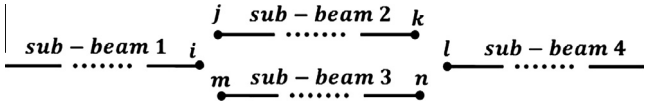

Figure 5 Nodes at the delamination boundaries.

where $N_i(\xi)$, with $i = 1$–3, are the Lagrangian interpolation or shape functions associated with node i given by [24]

$$N_1(\xi) = 1 - 3\xi + 2\xi^2, \quad N_2(\xi) = 4(\xi - \xi^2),$$
$$N_3(\xi) = 2\xi^2 - \xi \tag{6}$$

where $\xi = x/L_e$ and L_e is the element length of the beam. The vector of element degrees of freedom $\{\delta\}$ is given by

$$\{\delta\} = \{u_1, w_1, \psi_{x1}, \psi_{y1}, u_2, w_2, \psi_{x2}, \psi_{y2}, u_3, w_3, \psi_{x3}, \psi_{y3}\}^T \tag{7}$$

where the superscript T denotes the transpose of a vector or a matrix.

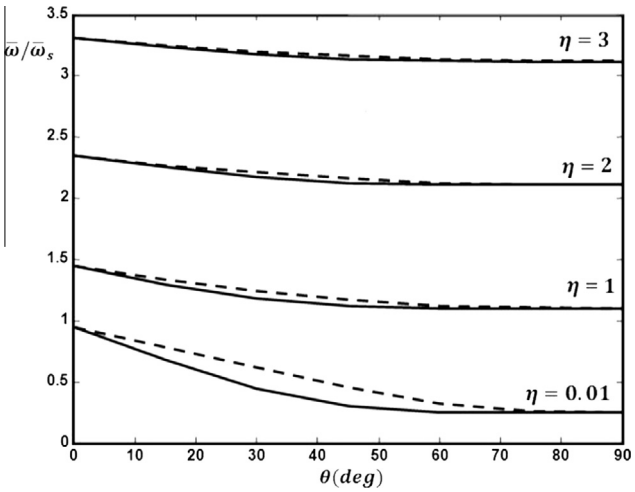

Figure 6 Effect of angle of orientation and rotating speed on the fundamental frequency ($L/h = 15$) (Solid Line: WPE; Dashed Line: WOPE).

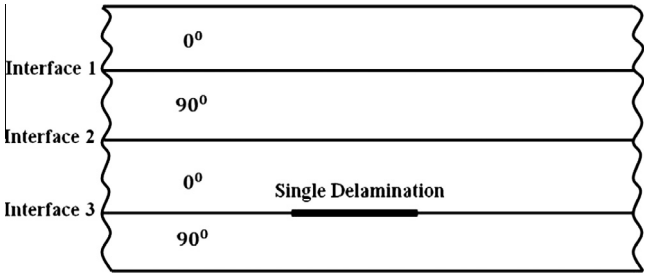

Figure 7 A LCB with [0/90/0/90] layups and a central delamination ($L/h = 15$).

The displacements and rotations of the beam can be related to the nodal degrees of freedom throughout the use of the shape functions to give

$$\begin{aligned} u &= \lfloor N_u \rfloor \{\delta\} = \lfloor N_1, 0, 0, 0, N_2, 0, 0, 0, N_3, 0, 0, 0 \rfloor \{\delta\} \\ w &= \lfloor N_w \rfloor \{\delta\} = \lfloor 0, N_1, 0, 0, 0, N_2, 0, 0, 0, N_3, 0, 0 \rfloor \{\delta\} \\ \psi_x &= \lfloor N_{\psi_x} \rfloor \{\delta\} = \lfloor 0, 0, N_1, 0, 0, 0, N_2, 0, 0, 0, N_3, 0 \rfloor \{\delta\} \\ \psi_y &= \lfloor N_{\psi_y} \rfloor \{\delta\} = \lfloor 0, 0, 0, N_1, 0, 0, 0, N_2, 0, 0, 0, N_3 \rfloor \{\delta\} \end{aligned} \tag{8}$$

One of the efficient ways of deriving dynamic characteristics of a system using FEM is to employ the energy principle [4,24]. In implementing this method, one has to derive the kinetic and potential energies of the system, which will be presented in the following sections.

2.4. Stiffness and mass matrices of the element

To obtain the stiffness matrix of the beam element, we start by substituting the Eq. (8) in Eq. (3) to get the following expression for the stiffness matrix [4,24]:

$$U = \frac{1}{2}\{\delta\}^T [K^e] \{\delta\} \tag{9}$$

where the element stiffness matrix is given by

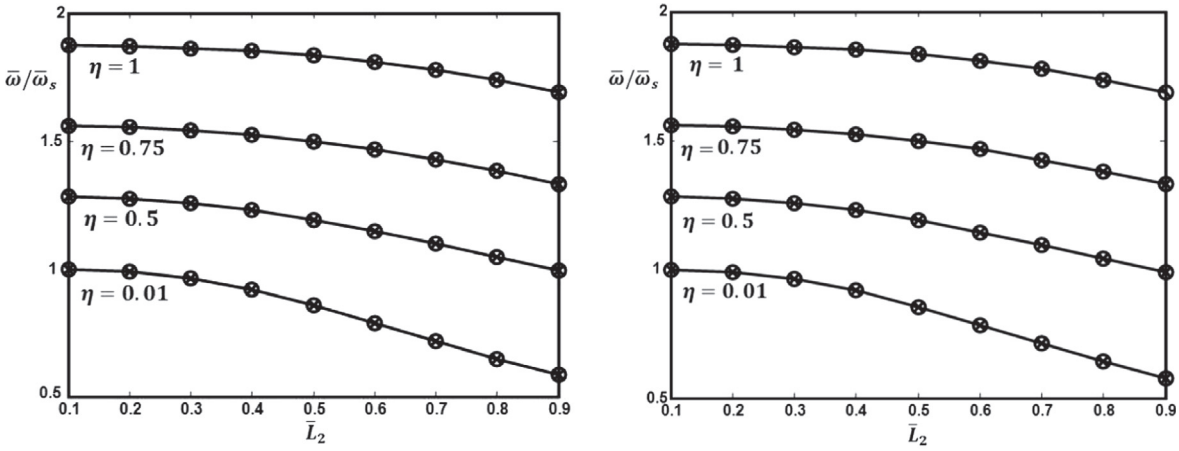

(a) Delamination located at interface 1

(b) Delamination located at interface 2

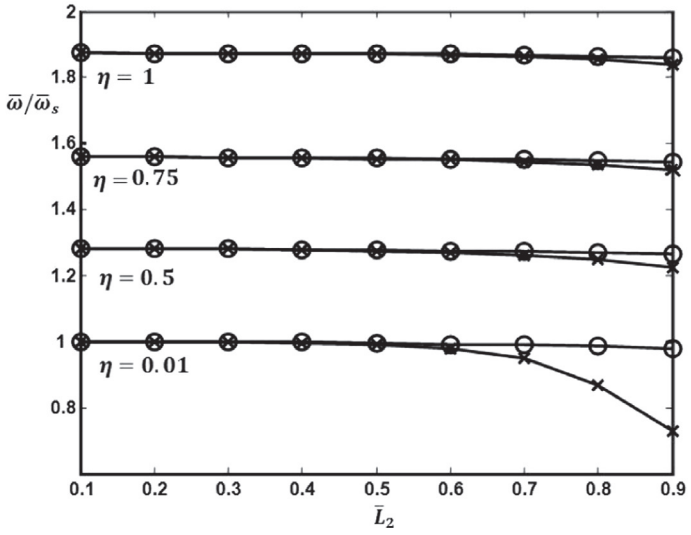

(c) Delamination located at interface 3

Figure 8 The influence of thicknesswise location and delamination length on the natural frequencies for different rotating speeds (Free Mode: —×—; Constrained Mode: —○—).

$$
\begin{aligned}
[K^e] = & \int_0^1 \left[\overline{A}_{11}\lfloor N_{u,x}\rfloor^T\lfloor N_{u,x}\rfloor + \overline{B}_{11}\lfloor N_{u,x}\rfloor^T\lfloor N_{\psi_x,x}\rfloor + \overline{B}_{11}\lfloor N_{\psi_x,x}\rfloor^T\lfloor N_{u,x}\rfloor\right] L_e d\xi \\
& + \int_0^1 \left[\overline{B}_{16}\lfloor N_{u,x}\rfloor^T\lfloor N_{\psi_y,x}\rfloor + \overline{B}_{16}\lfloor N_{\psi_y,x}\rfloor^T\lfloor N_{u,x}\rfloor + \overline{D}_{11}\lfloor N_{\psi_x,x}\rfloor^T\lfloor N_{\psi_x,x}\rfloor\right] L_e d\xi \\
& + \int_0^1 \left[\overline{D}_{16}\lfloor N_{\psi_x,x}\rfloor^T\lfloor N_{\psi_y,x}\rfloor + \overline{D}_{16}\lfloor N_{\psi_y,x}\rfloor^T\lfloor N_{\psi_x,x}\rfloor + \overline{D}_{66}\lfloor N_{\psi_y,x}\rfloor^T\lfloor N_{\psi_y,x}\rfloor\right] L_e d\xi \\
& + \int_0^1 \left[\overline{A}_{55}(\lfloor N_{\psi_x}\rfloor^T\lfloor N_{\psi_x}\rfloor + \lfloor N_{\psi_x}\rfloor^T\lfloor N_{w,x}\rfloor + \lfloor N_{w,x}\rfloor^T\lfloor N_{w,x}\rfloor + \lfloor N_{w,x}\rfloor^T\lfloor N_{\psi_x}\rfloor)\right] L_e d\xi \\
& + I_1\Omega^2 \int_0^1 \left[(r_0 L + L^2/2 - r_0 L_s - L_s^2/2) - (r_0 + L_s)L_e\xi - (L_e\xi)^2/2\right]\lfloor N_{w,x}\rfloor^T\lfloor N_{w,x}\rfloor L_e d\xi
\end{aligned}
\tag{10}
$$

and L_s which is in the last term in Eq. (10) is the beam element location in the axial direction, as shown in Fig. 4

On the other hand, by substituting Eq. (8) in Eq. (1) and integrating over the element length, the element mass matrix is derived as

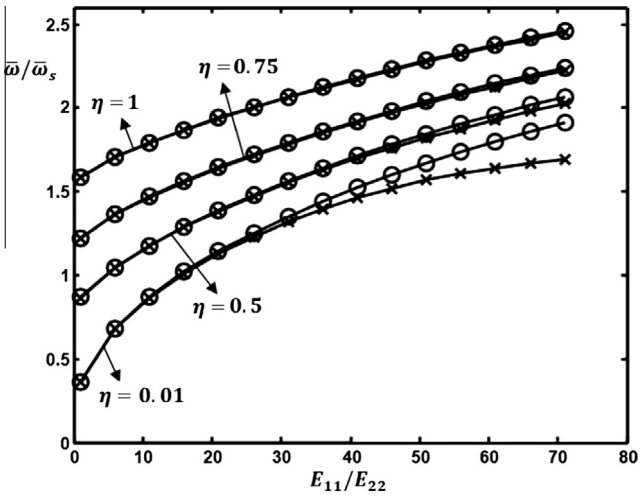

Figure 9 Effect of material anisotropy and rotating speed on the fundamental frequency (Free Mode: —×—; Constrained Mode: —○—).

$$T = \frac{1}{2}\{\delta\}^T[M^e]\{\delta\} \tag{11}$$

where the element mass matrix is

$$[M^e] = \int_0^1 \left[I_1\left(\lfloor N_u\rfloor^T\lfloor N_u\rfloor + \lfloor N_w\rfloor^T\lfloor N_w\rfloor\right) + I_3\left(\lfloor N_{\psi_x}\rfloor^T\lfloor N_{\psi_x}\rfloor + \lfloor N_{\psi_y}\rfloor^T\lfloor N_{\psi_y}\rfloor\right)\right] L_e d\xi \tag{12}$$

2.5. Displacement continuity conditions

The displacement continuity conditions have to be satisfied at the junction between the undelaminated segment sub-beam 1 and the delaminated segments sub-beam 2 and sub-beam 3, and similarly at the junction between the undelaminated segment sub-beam 4 and the delaminated segments sub-beams 2 and 3. Considering the whole beam's elements at the connecting nodes i, j, k and l for sub-beams 1, 2 and 4, as shown in Fig. 5, the overall element nodal displacement vectors and the stiffness and mass matrices of sub-beams 1–4 are $\{\Delta\}_i$, $[K]_i$ and $[M]_i$ (i = 1, 2, 3, 4), respectively.

At the connection nodes i–j and k–l, the displacement continuity conditions are as follows:

$$\begin{aligned} &u|_{node\,j} = (u - e_2\psi_x)|_{node\,i}, \quad w|_{node\,j} = w|_{node\,i}, \quad \psi_x|_{node\,j} = \psi_x|_{node\,i}, \quad \psi_y|_{node\,j} = \psi_y|_{node\,i} \\ &u|_{node\,k} = (u - e_2\psi_x)|_{node\,l}, \quad w|_{node\,k} = w|_{node\,l}, \quad \psi_x|_{node\,k} = \psi_x|_{node\,l}, \quad \psi_y|_{node\,k} = \psi_y|_{node\,l} \end{aligned} \tag{13}$$

where e_2 is the distance between the mid-planes of the sub-beams 1 and 2. The following transformation relations for the element stiffness and mass matrices can be established [4,24]:

$$\begin{aligned} [\overline{K}]_2 &= [T_1]^T[K]_2[T_1] \\ [\overline{M}]_2 &= [T_1]^T[M]_2[T_1] \end{aligned} \tag{14}$$

Assuming the dimension $c_1 \times c_1$ for the stiffness and mass matrices of sub-beam 2 and based on the Eq. (13), the transformation matrix T_1 has the dimension of $c_1 \times c_1$ and is given as

All $T_1(i, j) = 0$ except;

$$\begin{cases} T_1(i,j) = 1 \quad i = j \\ T_1(1,3) = -e_2 \\ T_1(c_1 - 3, c_1 - 1) = -e_2 \end{cases} \tag{15}$$

A similar treatment can be carried out for the connection nodes i–m and n–l and the following transformation relations for the element stiffness and mass matrices can be established:

$$\begin{aligned} [\overline{K}]_3 &= [T_2]^T[K]_3[T_2] \\ [\overline{M}]_3 &= [T_2]^T[M]_3[T_2] \end{aligned} \tag{16}$$

in which the transformation matrix T_2 has the dimension of the stiffness and mass matrices of sub-beam 3 (i.e. $c_2 \times c_2$) and is given as

All $T_2(i, j) = 0$ except

$$\begin{cases} T_2(i,j) = 1 \quad i = j \\ T_2(1,3) = e_3 \\ T_2(c_2 - 3, c_2 - 1) = e_3 \end{cases} \tag{17}$$

where e_3 is the distance between the mid-planes of the sub-beams 1 and 3. The matrices $[\overline{K}]_i$ and $[\overline{M}]_i$ $(i = 2, 3)$ are used to assemble the total stiffness and mass matrices.

3. Eigenvalue equations

Based on the procedure outlined in the previous sections, the total equation of motion for the delaminated beam is

$$[M]\{\Delta\}_{,tt} + [K]\{\Delta\} = \{0\} \tag{18}$$

where $[K]$ and $[M]$ are the total stiffness and mass matrices, respectively, after applying the boundary conditions. Assuming a general solution $\{\Delta\} = \{\Delta_0\}e^{i\omega t}$ for the Eq. (18), and taking $\omega^2 = \lambda$, we obtain

$$|[K] - \lambda[M]|\{\Delta_0\} = \{0\} \tag{19}$$

where ω is the natural frequency and $\{\Delta_0\}$ is the corresponding mode shape. The nontrivial solutions for the Eq. (19) can be obtained by solving equation $\det([K]–\lambda[M]) = 0$, which then yields the eigenvalues of the system ($\omega_i^2 = \lambda_i$).

4. Numerical results and discussion

The natural frequencies obtained from the FE model of the LCB are compared with the experimental and theoretical results presented by other investigators in order to demonstrate the accuracy of the present FE model. The verification and validation of the present model, which are presented in

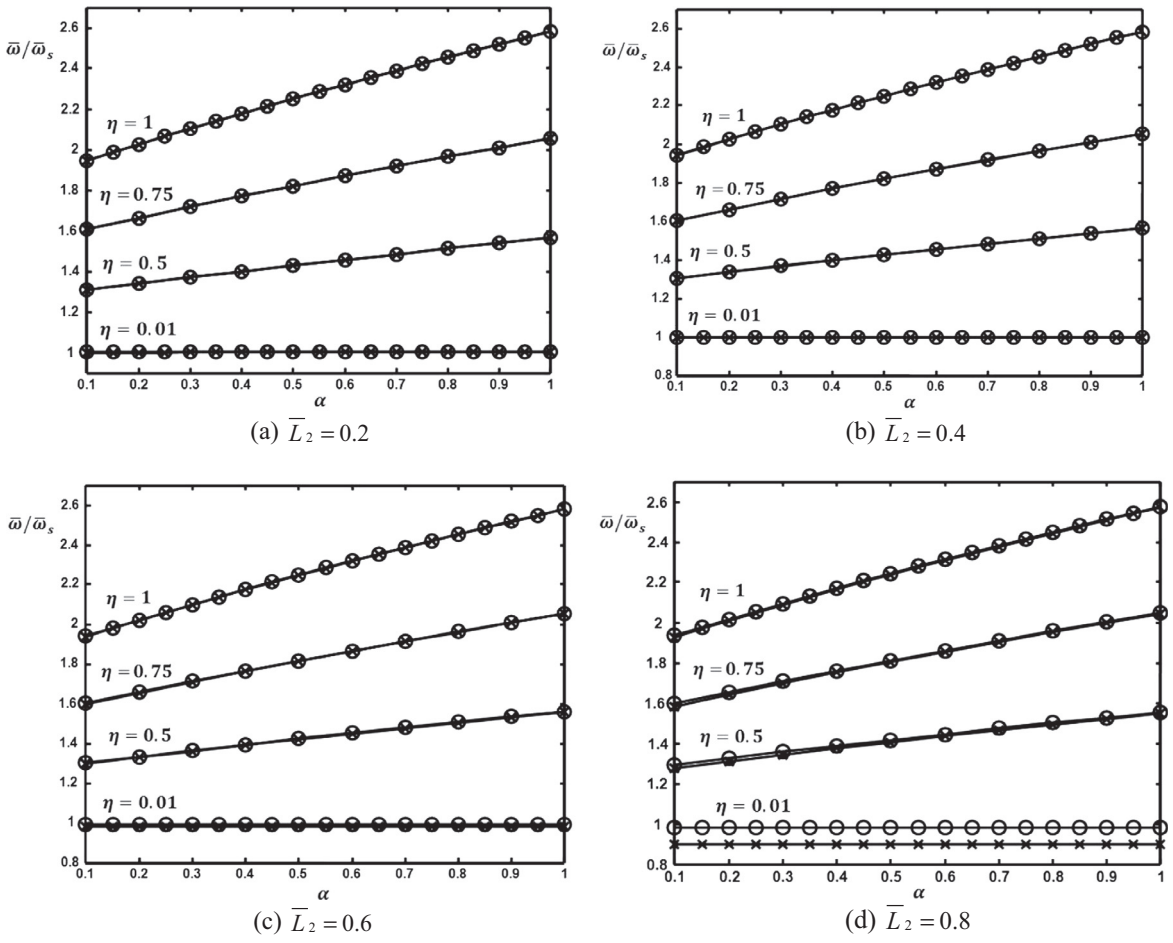

Figure 10 The influence of hub radius on the natural frequencies (Free Mode: —×—; Constrained Mode: —○—).

Section 4.1 consist of two parts: part one consists of a convergence study to be able to determine the suitable number of elements that will be used in the FE model and then verify the results of the present model with published results on rotating intact (undelaminated) beam; and part two consists of verifying and validating the results of the present model with published analytical and experimental data on non-rotating intact/delaminated beam. The study on the vibration characteristics of the rotating delaminated beam is presented in Section 4.2.

Unless mentioned otherwise, the numerical results are presented for AS4/3501 Graphite-Epoxy LCB with the following mechanical properties [1]:

$$E_{11} = 144.8\ \text{GPa}, \quad E_{22} = 9.65\ \text{GPa}, \quad G_{12} = 4.14\ \text{GPa},$$
$$G_{13} = 4.14\ \text{GPa},$$
$$G_{23} = 3.45\ \text{GPa}, \quad \upsilon_{12} = 0.33, \quad \rho = 1389.23\ \text{kg/m}^3 \tag{20}$$

In all subsequent problems the width of the beam is taken as unity, the thickness of all layers in the LCB is equal and the shear correction factor is taken to be $k_s = 5/6$ [1]. The shear correction factor has been used to calculate the shear stiffness $\overline{A}_{55}$ in Eq. (3). Also, the calculated natural frequencies in these examples are presented in a dimensionless form $\bar{\omega}$.

4.1. Verification and validation

The convergence analysis is conducted for non-rotating intact LCB by setting the rotational speed to zero. The dimensionless fundamental natural frequencies of symmetric laminated angle-ply beams $[\theta/-\theta]_S$ are compared with the analytical solutions presented in Refs. [5] and [25]. As shown in Table 1, the natural frequencies for the delaminated beam that are obtained from Eq. (19) converge to the exact values as the number of elements increases. It is worth mentioning that all of the results in this paper use the 50 beam elements in the discretized model to obtain the converged results. As the angle of orientation increases from 0° to 90°, the dimensionless fundamental frequency decreases. The present angle-ply results are in good agreement with Ref. [5] but deviate from the results presented in Ref. [25]. This is due to the fact that the laminated beam theory considered in Ref. [25] neglects Poisson's effect. Moreover, the material couplings have been considered partially in Ref. [25]. These lead to significant error in the analysis of beams with angle-ply layups especially for the layout angle between 30° and 60° [1–5,16,17].

The first non-dimensional natural frequencies of a clamped-free rotating intact beam based on the Timoshenko beam theory are compared with the analytical results of Du et al. [20]

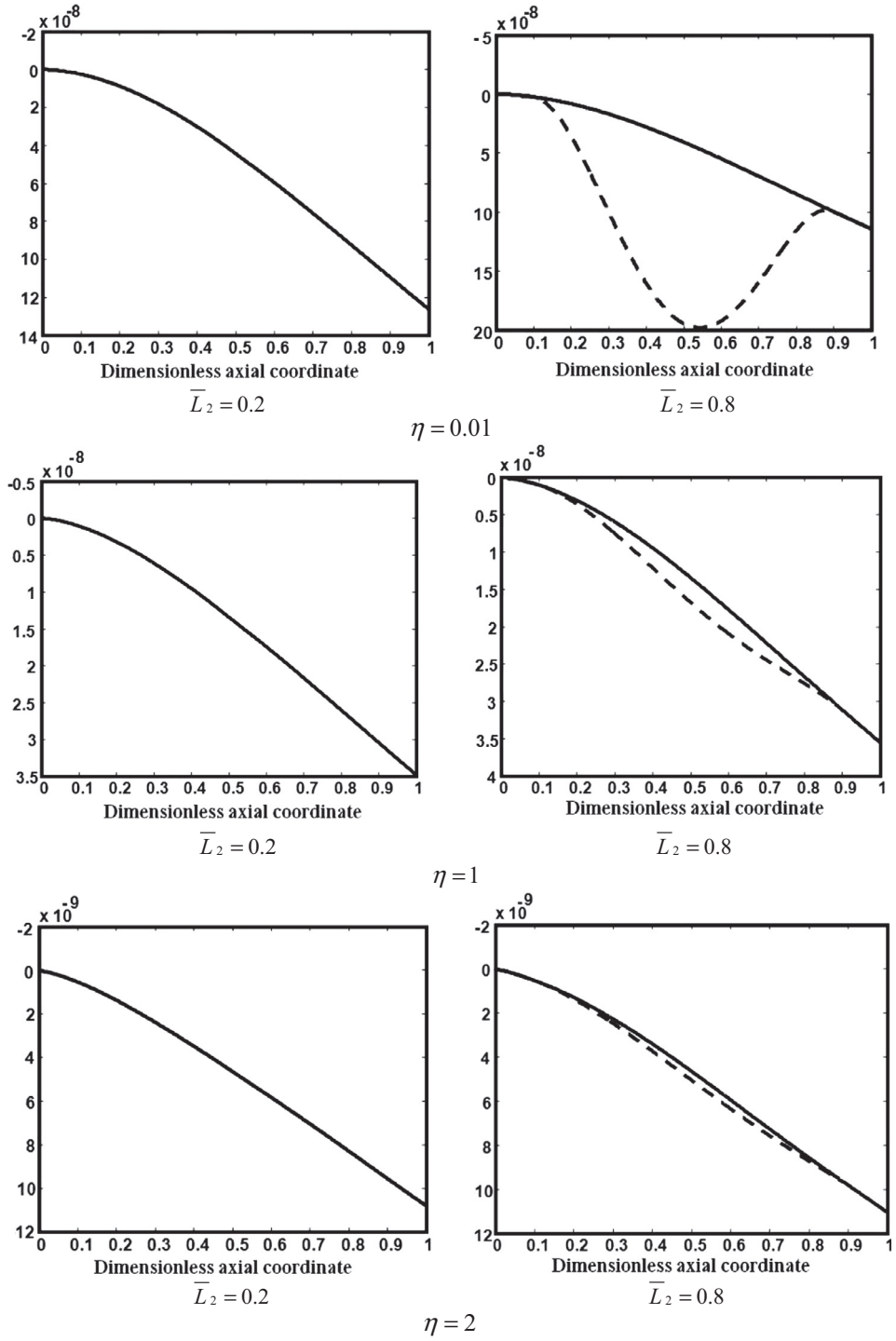

Figure 11 First mode shape of a rotating LCB with delamination located at interface 3 for two different lengths and five different rotating speeds.

and Liu and Shu [23]. For the purpose of comparison, the dimensionless parameters $\bar{\omega}'$ and η' are considered for natural frequency and rotating speed, respectively. Moreover, the effect of Timoshenko beam theory is represented by $r = R/L$, where R is the radius of gyration. Table 2 shows good agreement between the present results and the results that are published in the literature [20,23].

The first verification and validation of the present FE model on a delaminated beam are performed by comparing the results of the present model with published experimental data [26] and analytical results [27] on a delaminated non-rotating beam with clamped-free boundary conditions. The laminated beam is an eight-ply $[0/90/90/0]_s$ Glass-Epoxy beam and is 266.7 mm long, 25.4 mm wide and 1.778 mm thick. The

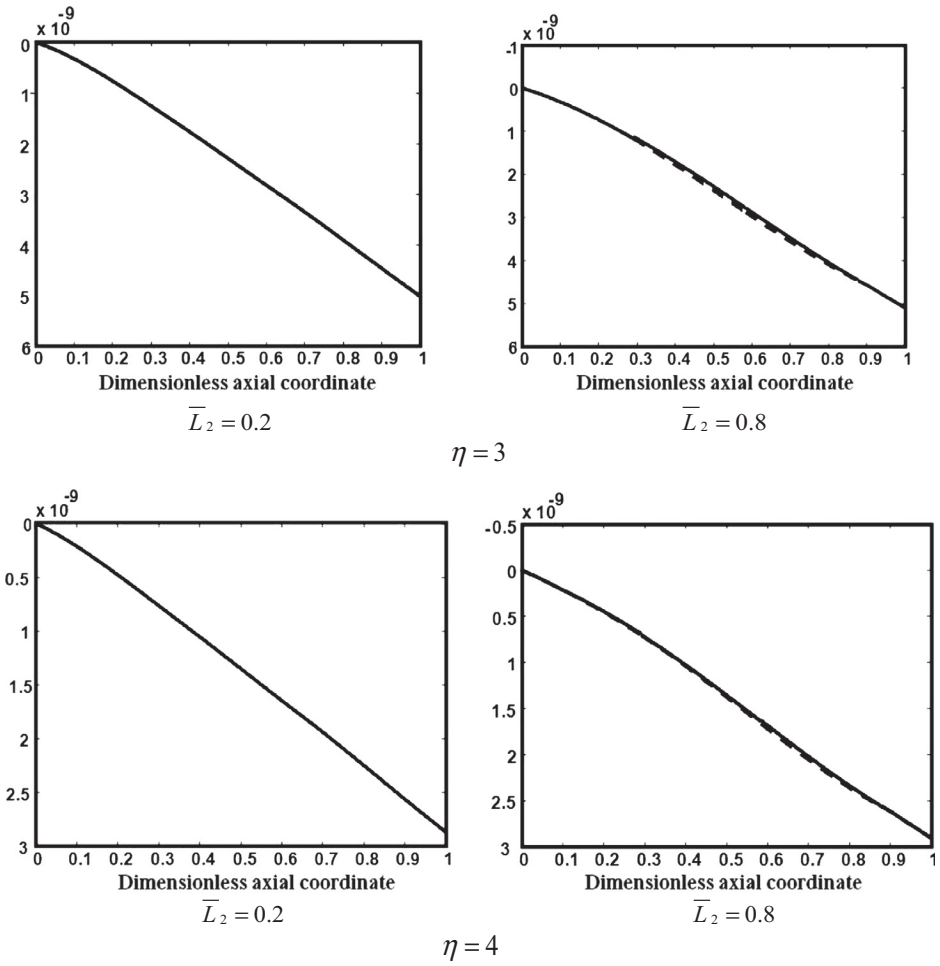

Fig. 11 (*continued*)

material properties are given in Ref. [27]. The distance between the center of the delamination and the clamped end is 117.5 mm. Table 3 presents the results for a 101.6-mm mid-plane delamination. It should be noted that when the delaminations are located at the mid-plane of the LCB, the frequencies predicted by the 'free mode' and the 'constrained mode' are identical, which have also been observed in previous studies [9–11,27]. It can be seen that the present results are in good agreement with the published analytical and experimental data.

The second verification and validation consider an eight-ply T300/934 graphite/epoxy cantilever LCB with layups of [0/90/0//90/90/0/90/0] and dimensions of $127 \times 12.7 \times 1.016\ \text{mm}^3$. The material properties are adopted from Ref. [8]. The delamination is centrally located, and four normalized delamination lengths, 0.2, 0.4, 0.6 and 0.8, are considered. Table 4 shows a good agreement between the present "free mode" and "constrained mode" fundamental frequencies of the delaminated LCB with the experimental data [8] and analytical results [28] that are presented in the literature.

From these comparisons, an assurance is given that the developed program is working properly; hence, in the next section analysis is further pursued on the dynamic behavior of rotating delaminated LCB.

4.2. Results for rotating delaminated beam

Fig. 6 shows the effects of the angle of orientation of the fibers, θ, and the rotating speed, η, on the non-dimensional frequency of the rotating delaminated beam, ω/ω_s, based on the free mode model. In this figure, ω is the natural frequency of the rotating delaminated beam and ω_s is the natural frequency of the non-rotating intact beam. Furthermore, the value of ω_s is calculated for $\theta = 0°$. The Poisson effect is also considered here, where WPE and WOPE stand for the case with and without the Poisson's effects, respectively. A delaminated beam with layups $[\theta/-\theta/-\theta//\theta]$ and central delamination with dimensionless length $\overline{L}_2 = 0.2$ is considered here. The double slash "//" is used to indicate the thicknesswise location of the delamination. Similarly with the results presented in Table 1, the natural frequency ω/ω_s decreases as the angle of orientation θ increases from 0° to 90°. As expected, the Poisson's effect produces no significant changes on the fundamental frequency for the unidirectional ($\theta = 0°$) or cross-ply ($\theta = 90°$) LCB. However, the fundamental frequency for an angle-ply beam where Poisson's effect is not considered deviates significantly from the exact value (i.e. considering Poisson's effect), especially if layout angle is between 30° and

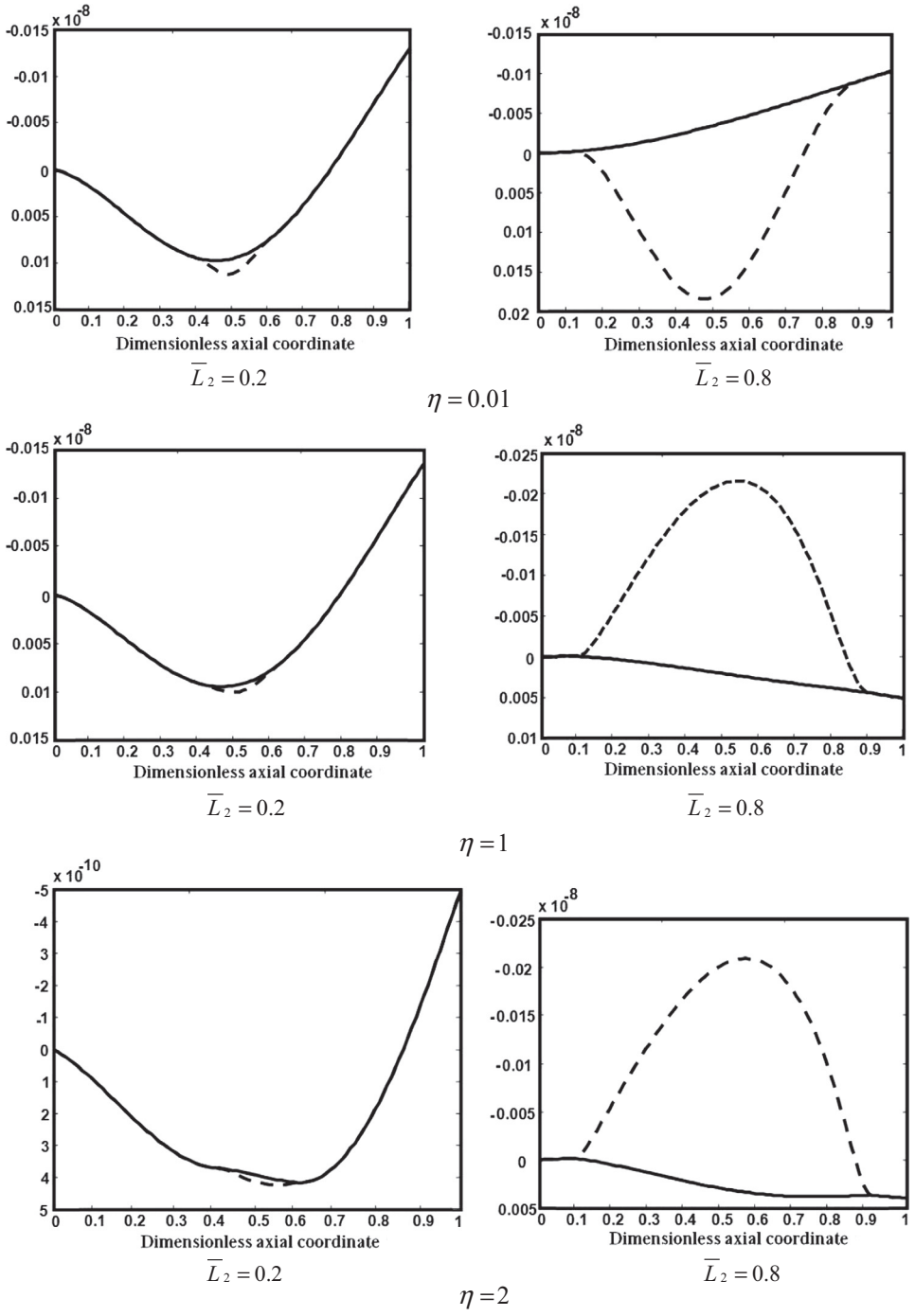

Figure 12 Second mode shape of a rotating LCB with delamination located at interface 3 for two different lengths and five different rotating speeds.

60°. Note that the difference between WPE and WOPE decreases as the rotating speed increases. Fig. 6 also shows that natural frequency increases as the rotating speed η increases which is due to the stiffening effect of the rotating beam.

Now we consider a beam comprised of four laminas with layups shown in Fig. 7. The effect of thicknesswise location and delamination length on the dynamic response of the LCB is depicted in Fig. 8. Based on the results, the natural frequency ω/ω_s decreases as the delamination length $\overline{L}_2$ increases. Furthermore, when the delamination is located at interface 1 or 2, the natural frequencies of the beam using the free mode and constrained mode are almost the same, that is no "opening" is seen. But when the delamination is located at interface 3, the difference between the results of the free mode and the constrained mode increases as the delamination length increases and this difference increases more as the rotating speed decreases. When the delamination is located at interface 1 the bending stiffness of sub-beams [0] and the [90/0/90] is almost the same, whereas, when the delamination is located at interface 3, the difference between the bending stiffness

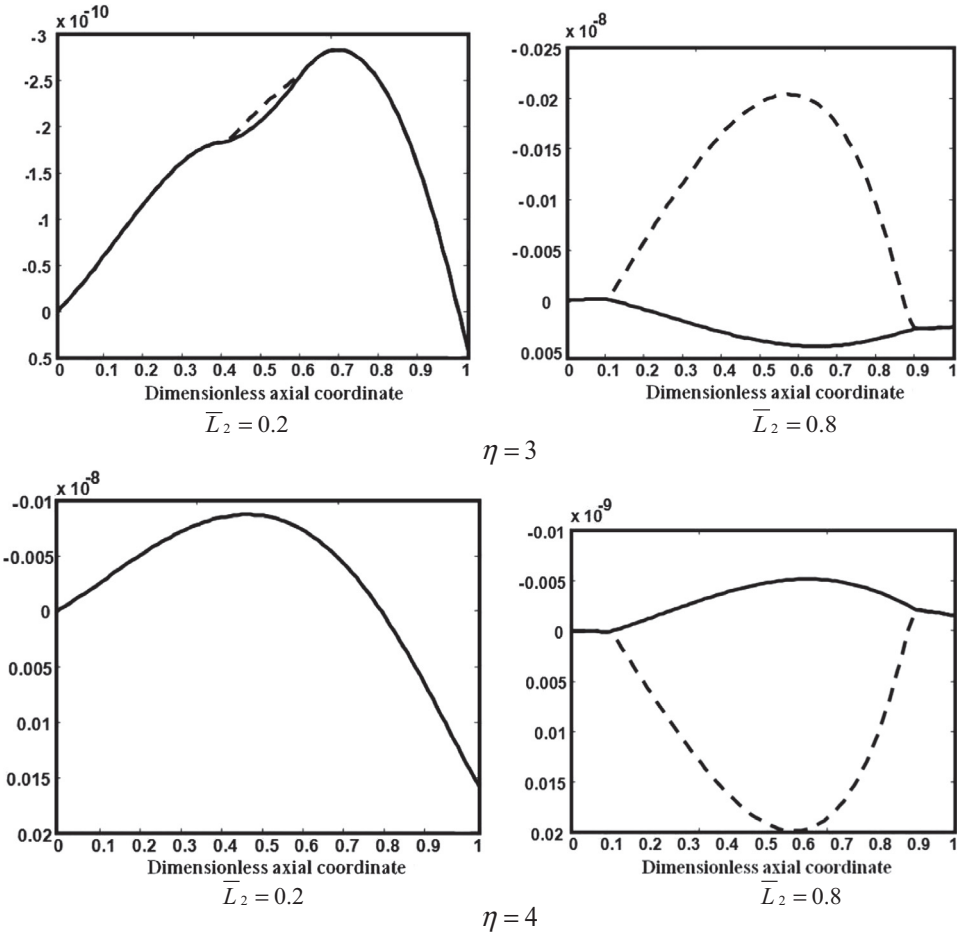

Fig. 12 (*continued*)

values of the clustered sub-beam 2 with [0/90/0] layups and sub-beam 3 with [90] layup becomes relatively high. This indicates that the difference between the bending stiffness of the sub-beams in the delamination region significantly affects the difference between the free and constrained mode frequencies. Fig. 8(c) further shows the natural frequencies obtained from the free mode model represent the lower bound and the constrained mode model signifies the upper bound of the exact solutions, which have been mentioned in previous studies [9–13].

Fig. 9 shows the effect of material anisotropy on the first non-dimensional frequencies of the rotating delaminated beam. In this case again we take a central delamination with $\overline{L}_2 = 0.6$ located at the interface 3 with beam slenderness ratio of $L/h = 15$. The layup configuration and thicknesswise location of the delamination, as shown in Fig. 7 are also considered in all of the following examples. Fig. 9 shows the effect of material anisotropy on the first natural frequency of the delaminated beam. The value of E_{11} is varied, while the other elastic constants are the same as those of AS4/3501 Graphite-Epoxy material presented in relation (20). It should be said that in calculating $\bar{\omega}$, $\bar{\omega}_s$ the value of $E_{11} = 144.8$ GPa is used. As it is shown the effect of increasing material anisotropy is to increase the natural frequencies of the beam. Moreover, it can be concluded that the differences of natural frequency between the constrained mode and the free mode assumptions decrease when rotating speed becomes higher.

Fig. 10 shows the normalized fundamental frequency of the LCB with a single central delamination versus α. This represents the influence of hub radius on the natural frequency of beams with a single delamination for delamination lengths $\overline{L}_2 = 0.2, 0.4, 0.6, 0.8,$. For high rotating speed, the natural frequency increases as the hub radius increases. However, for low rotating speed $\eta = 0.01$, the natural frequency is almost constant for different hub radius ratios. For long delamination (Fig. 10(c) and (d)), the difference between natural frequencies based on the free and constrained modes becomes smaller as rotating speed increases. It shows that the opening of the delaminated layers becomes negligible with a large rotating speed. The reason for the trend of natural frequencies for different parameters is due to the increase of stiffnesses of the sub-beams caused by the centrifugal force.

The first and second mode shapes of a thick LCB ($L/h = 15$) with a delamination located at Interface 3 and based on the free mode model are shown in Figs. 11 and 12. Two delamination lengths $\overline{L}_2 = 0.2$ and 0.8 and five rotating speeds $\eta = 0.01, 1, 2, 3, 4$ are considered. In the delaminated region, solid and dashed lines represent the amplitude of sub-beams 2 and 3, respectively. In these two figures, vertical axis indicates the normalized deflection for each point of the delaminated beam. For the considered beam, the corresponding dimensionless natural frequencies have been presented in Table 5. The opening in the mode shapes using the free mode

explains the difference between the constrained and free mode frequencies. For a large opening, the difference between the two frequencies is large, whereas for a small opening, the difference between the two frequencies is small. From these results, we can see that the first and second modes of such beam do not show significant opening in the cases when the rotating speed increases. It should be noted that this difference is significant for long delamination length and small rotating speed. The opening modes can also explain the difference between the "free mode" and "constrained mode" frequencies that are presented in Figs. 8–10, where the opening in the delaminated region cannot be seen when the beam is subjected to a bigger centrifugal force. This phenomenon is physically admissible.

5. Conclusions

In this paper, a finite element model for a rotating composite beam with a through-width delamination is presented. The model includes the rotary inertia and transverse shear effects, as well as material coupling effects. Parametric studies have been conducted to study the effects of the speed of rotation, delamination length and locations, material anisotropy and beam hub radius on the vibration characteristics of the beam. Based on the results the following conclusions are made:

1. The beam with delamination experiences reduction in natural frequencies due to the loss of stiffness and this reduction is more significant as the delamination length increases. However, as the rotating speed increases the natural frequency increases that is due to the stiffening of the sub-beams caused by the centrifugal force.
2. The thicknesswise location of the delamination has considerable effect on the vibrational characteristics of the delaminated beam. Indeed, when the stiffness of sub-beams 2 and 3 is close to each other, there is no significant delamination opening and closing during the vibration and hence the free and constrained modes predict the same values for natural frequencies.
3. The difference between frequencies based on the free and constrained modes is not affected by changing the hub radius. In other words, if the opening phenomenon is seen in the vibrational motion of the delaminated region, the hub radius does not have any influence on it.
4. It is observed that by increasing the rotating speed the free and constrained modes predict the same values for natural frequencies and therefore the opening between sub-beams 2 and 3 is not seen.

References

[1] Krishnaswamy S, Chandrashekhara K, Wu WZB. Analytical solutions to vibration of generally layered composite beams. J Sound Vib 1992;159(1):85–99.

[2] Kadivar MH, Mohebpour SR. Forced vibration of unsymmetric laminated composite beams under the action of moving loads. Compos Sci Technol 1998;58:1675–84.

[3] Ahmadian MT, Jafari-Talookolaei RA, Esmailzadeh E. Dynamics of a laminated composite beam on Pasternak viscoelastic foundation subjected to a moving oscillator. J Vib Control 2008;14(6):807–30.

[4] Jafari-Talookolaei RA, Kargarnovin MH, Ahmadian MT. Free vibration analysis of cross-ply layered composite beams with finite length on elastic foundation. Int J Comput Methods 2008;5(1):21–36.

[5] Jafari-Talookolaei RA, Abedi M, Kargarnovin MH, Ahmadian MT. An analytical approach for the free vibration analysis of generally laminated composite beams with shear effect and rotary inertia. Int J Mech Sci 2012;65:97–104.

[6] Wang JTS, Liu YY, Gibby JA. Vibrations of split beams. J Sound Vib 1982;84(4):491–502.

[7] Mujumdar PM, Suryanarayan S. Flexural vibrations of beams with delaminations. J Sound Vib 1988;125(3):441–61.

[8] Shen MHH, Grady JE. Free vibrations of delaminated beams. AIAA J 1992;30(5):1361–70.

[9] Shu D, Della CN. Free vibration analysis of composite beams with two nonoverlapping delaminations. Int J Mech Sci 2004;46:509–26.

[10] Della CN, Shu D. Free vibration analysis of composite beams with overlapping delaminations. Eur J Mech A/Solids 2005;24:491–503.

[11] Della CN, Shu D. Vibration of beams with two overlapping delaminations in prebuckled states. Compos Part B: Eng 2007;38:109–18.

[12] Della CN, Shu D. Vibration of beams with double delaminations. J Sound Vib 2005;282:919–35.

[13] Della CN, Shu D. Vibration of delaminated multilayer beams. Compos Part B: Eng 2006;37:227–36.

[14] Parlapalli MR, Shu D. Buckling analysis of two-layer beams with an asymmetric delamination. Eng Struct 2004;26(5):651–8.

[15] Rodman U, Saje M, Planinc I, Zupan D. Exact buckling analysis of composite elastic columns including multiple delamination and transverse shear. Eng Struct 2008;30(6):1500–14.

[16] Jafari-Talookolaei RA, Kargarnovin MH, Ahmadian MT. Dynamic response of a delaminated composite beam with general lay-ups based on the first-order shear deformation theory. Compos Part B: Eng 2013;55:65–78.

[17] Kargarnovin MH, Ahmadian MT, Jafari-Talookolaei RA, Abedi M. Semi-analytical solution for the free vibration analysis of generally laminated composite Timoshenko beams with single delamination. Compos Part B: Eng 2013;45:587–600.

[18] Kuo YH, Wu TH, Lee SY. Bending vibrations of a rotating non-uniform beam with tip mass and an elastically restrained root. Compos Struct 1992;42(2):229–36.

[19] Khulief YA, Bazoune A. Frequencies of rotating tapered Timoshenko beams with different boundary conditions. Compos Struct 1992;42(5):781–95.

[20] Du H, Lim MK, Liew KM. A power series solution for vibration of a rotating Timoshenko beam. J Sound Vib 1994;175:505–23.

[21] Su H, Jackson DR, Banerjee JR. Free vibration of rotating tapered beams using the dynamic stiffness method. J Sound Vib 2006;298:1034–54.

[22] Das SK, Ray PC, Pohit G. Free vibration analysis of a rotating beam with nonlinear spring and mass system. J Sound Vib 2007;301:165–88.

[23] Liu Y, Shu DW. Free vibration analysis of rotating Timoshenko beams with multiple delaminations. Compos Part B: Eng 2013;44:733–9.

[24] Zienkiewicz OC. The finite element method. London: McGraw-Hill; 1977.

[25] Chandrashekhara K, Krishnamurthy K, Roy S. Free vibration of composite beams including rotary inertia and shear deformation. Compos Struct 1990;14:269–79.

[26] Okafor A, Chandrashekhara K, Jiang YP. Smart Mater Struct 1996;5:338–47.

[27] Valoor MT, Chandrashekhara K. Compos Sci Technol 2000;60:1773–9.

[28] Luo H, Hanagud S. Dynamics of delaminated beams. Int J Solids Struct 2000;37:1501–19.

Ramazan-Ali Jafari-Talookolaei is the assistant professor at the School of Mechanical Engineering, Babol Noshirvani University of Technology. He received his B.Sc. in Mechanical Engineering from Shahrood University of Technology in 2002 with first rank, his M.Sc. and Ph.D. degrees in Mechanical Engineering from Sharif University of Technology, the best university in I.R.IRAN, in 2004 and 2013, respectively. His research interests include Laminated Composite Structures, Finite Element Method, Dynamics, Vibration, Linear and Non-linear Analysis, Damaged Structures, Analytical Solutions. He has published more than 20 journal papers, 15 conference papers and 3 books. His PhD thesis has been selected as the best PhD thesis in the field of Acoustics and Vibration defended during September 2011- September 2013 in I.R.IRAN, Selected by Iranian Society of Acoustics and Vibration (ISAV), ISAV 3rd Conference, 25-26 December 2013.

Christian N. Della is currently an assistant professor at the University of Glasgow Singapore. He obtained his BSc in Mechanical Engineering from Saint Louis University (SLU), Philippines, MSc Mechanical Engineering from the University of the Philippines-Diliman, and PhD from the School of Mechanical and Aerospace Engineering at Nanyang Technological University (NTU), Singapore. His current research interests include dynamics, composite material structures, piezoelectric composites, solid mechanics, and computational mechanics. He has published over 30 journal and conference papers.